Generalized Image Navigation & Registration Method Based on Kalman Filter

By Ahmed A. Kamel,[1] Handol Kim,[2] Dochul Yang,[2] Chul-Min Park,[3] and Jin Woo[4]

[1]Kamel Engineering Services, Los Angeles, California, USA;
[2]Korea Aerospace Research Institute, Daejeon, ROK;[3]Korea Aerospace Industries, ROK;
[4]Korea Meteorological Administration, Daebang-dong, ROK

A Generalized Image Navigation and Registration (INR) method using Kalman Filter (KF) is presented. The fundamental method is landmark-based, 'self-contained' INR system that estimates orbit or refines the coarse orbit received from the Flight Dynamics System (FDS). Kalman Filter measurement inputs consist of landmarks taken by the imaging instrument, maneuver delta v or orbit from FDS, and attitude from spacecraft telemetry inserted in the imager wideband data. The KF state vector (SV) consists of spacecraft attitude correction angles, constant attitude correction angles biases, spacecraft orbit position and velocity relative to ideal orbit, imager internal misalignments, and constant misalignment biases. The fundamental method is then shown how it can be adapted to systems using star and landmark measurements, systems using star only measurements with orbit provided by FDS or by the Global Positioning System (GPS), and systems using spacecraft attitude rate inserted in wideband telemetry.

Keywords: INR, Kalman Filter, Orbit Determination, Flight Dynamics

Nomenclature

R_{so}	: ideal geosynchronous radius = 42164000 meters
R_{eo}	: equatorial radius = 6378136.6 meters
f	: earth flattening=1/298.25642
ω_e	: sidereal earth rotation rate = 7.2921159E-05 rad/sec
λ_{so}	: ideal satellite longitude
h	: landmark altitude
S, C	: Sin, Cos
R, L, λ	: radius, geocentric latitude, longitude
ϕ, θ, ψ	: roll, pitch, yaw
LOS	: line of sight
LRF	: LOS reference frame
IIRF	: imager internal reference frame
ACF	: attitude control frame
ORF	: orbit reference frame
GEOS	: fixed grid frame
ECLF	: earth centered local frame
EW,NS	: East-West, North-South
$I_{ixi}, 0_{ixj}$	: ixi identity matrix, ixj null matrix

Subscripts

0, s, e	: initial, satellite, earth
T	: landmark point on earth
ma	: misalignment
m	: number of imager internal misalignment
att	: spacecraft attitude from telemetry
corr	: thermoelastic/attitude correction angles

1. Introduction

The term image navigation and registration and the INR acronym were coined by Kamel[1] and patented in US Patents # 4,688,091, 4,688,092, and 4,746,976 to represent a system that determines image pixel location and register it to fixed grid frame (called FGF in GOES and GEOS in COMS and in this paper). This INR invention became the foundation for subsequent GOES and similar systems worldwide[2-5]. The INR system requirements have been tightened as spacecraft and ground systems hardware has been improved[6-9].

The image navigation part of INR relates to determining LOS absolute pointing. Section 2 defines the INR and KF state vectors needed for this process. Section 3 describes new INR method (patent applications are being filed in ROK and in US) based on landmark measurements to determine orbit, attitude correction, and imager misalignments with maneuvers delta V provided by FDS. Also, orbit refinement can be made if FDS provides orbit with coarse accuracy instead of delta V. Section 4 shows the simulation results of this fundamental system. Section 5 shows how the new method can be adapted to be used for other INR system measurements implemented nowadays to improve INR performance.

The image registration part of INR relates to maintaining LOS stability. The objective of image registration is to provide the users with images with pixels that have the same fixed earth location regardless of time. Section 6 provides an algorithm for transferring pixels from LOS frame to GEOS frame needed for pixel data resampling in GEOS fixed grid frame.

2. INR and KF SV Definitions

2.1 INR SV definition

The INR SV is required for transformation from LRF to GEOS for section 3.1.2. This is given by:

$$SV_{INR} = [SV_{ma}^T \ SV_{corr}^T \ SV_{att}^T \ SV_{orb}^T]^T \qquad (1)$$

SV_{ma} is based on IIRF misalignment relative to LRF. SV_{corr}, SV_{att}, and SV_{orb} are based on:

$(\phi_{corr} \ \theta_{corr} \ \psi_{corr}) = $ ACF attitude relative to IIRF.
$(\phi_{att}, \theta_{att}, \psi_{att}) = $ ORF attitude relative to ACF.
$(\phi_{orb}, \theta_{orb}, \ \psi_{orb}) = $ GEOS attitude relative to ORF.

For single mirror imagers, such as in GOES I-P, COMS, MTSAT2, SV_{ma} is given by:

$$SV_{ma} = [\phi_{ma} \ \theta_{ma}]^T$$
$$= SV_{ma,model} + x_{ma} \qquad (2.1)$$

$$SV_{ma,model} = [\phi_{ma,model} \ \ \theta_{ma,model}]^T \qquad (2.2)$$

$$SV_{corr} = [\phi_{corr} \ \theta_{corr} \ \psi_{corr}]^T$$
$$= SV_{corr,model} + x_{corr} \qquad (3.1)$$

$$SV_{corr,model} = [\phi_{corr,model} \ \theta_{corr,model} \ \psi_{corr,model}]^T \quad (3.2)$$

The thermoelastic (also called thermal distortion) misalignment and correction models are computed in section 3.4 and (x_{ma}, x_{corr}) are defined in section 2.2 and determined by KF.

$$SV_{att} = [\phi_{att} \ \theta_{att} \ \psi_{att}]^T \text{ from telemetry} \qquad (4)$$

$$SV_{orb} = [R_s \ \ \Delta\lambda_s \ \ L_s \ ]^T \qquad (5.1)$$

$$R_s = R_{so}\left(1 + \frac{\Delta R_s}{R_{so}}\right), \ \Delta\lambda_s = \lambda_s - \lambda_{so} \qquad (5.2)$$

SV_{ORF} is given by:

$$SV_{ORF} = [\phi_{orb} \ \ \theta_{orb} \ \ \psi_{orb} \ ]^T \qquad (6.1)$$

For Spacecraft x axis parallel to earth equator (e.g., COMS) and using 3-1-2 type rotation:

$$SV_{ORF} = [L_s \ \Delta\lambda_s \ \ 0]^T \qquad (6.2)$$

For Spacecraft x axis parallel to orbit plane (e.g., GOES I-M) and using 3-1-2 type rotation:

$$SV_{ORF} = [L_s \ \Delta\lambda_s \ \ \dot{L}_s/\omega_e]^T \qquad (6.3)$$

$\left(\frac{\Delta R_s}{R_{so}}, \ \Delta\lambda_s, L_s, \dot{L}_s/\omega_e\right) = $ Kamel parameters[10-11] originally used for GOES I-M to represent actual orbit deviation from ideal orbit that is produced by a spherical earth and no luni-solar perturbations. In this paper, it is called ideal orbit refinement and it is determined by KF.

If FDS provides maneuver delta V:

$$\frac{\Delta R_s}{R_{so}} = \frac{\delta R_s}{R_{so}}, \Delta\lambda_s = \delta\lambda_s, \ L_s = \delta L_s, \dot{L}_s = \delta\dot{L}_s \qquad (7.1)$$

$(\frac{\delta R_s}{R_{so}}, \ \delta\lambda_s, \delta L_s, \delta\dot{L}_s) = $ Ideal orbit refinement by KF.

If FDS provides orbit instead of maneuver delta V:

$$\frac{\Delta R_s}{R_{so}} = \left[\frac{\Delta R_{FDS}}{R_{so}} + \frac{\delta R_s}{R_{so}}\right], \Delta\lambda_s = \Delta\lambda_{FDS} + \delta\lambda_s,$$

$$L_s = L_{FDS} + \delta L_s, \ \dot{L}_s = \dot{L}_{FDS} + \delta\dot{L}_s \qquad (7.2)$$

$(\frac{\delta R_s}{R_{so}}, \ \delta\lambda_s, \delta L_s, \delta\dot{L}_s) = $ FDS orbit refinement by KF.

2.2 KF SV definition

$SV_{KF} = x$ is needed to determine SV_{INR} of section 2.1. This is defined as follows:

$$x = [x_{corr}^T \ \dot{x}_{corr}^T \ x_{orb}^T \ \dot{x}_{orb}^T \ x_{ma}^T \ \dot{x}_{ma}^T]^T \qquad (8.1)$$

$$x_{corr} = [\delta\phi_{corr} \ \delta\theta_{corr} \ \delta\psi_{corr}]^T \qquad (8.2)$$

$$\dot{x}_{corr} = [b_{\phi_{corr}} \ b_{\theta_{corr}} \ b_{\psi_{corr}}]^T = \text{constant} \qquad (8.3)$$

$$x_{orb} = \left[\frac{\delta R_s}{Rso} \ \ \delta\lambda_s \ \ \delta L_s\right]^T \qquad (8.4)$$

$$\dot{x}_{orb} = \left[\frac{\delta\dot{R}_s}{Rso} \ \ \ \delta\dot{\lambda}_s \ \ \delta\dot{L}_s\right]^T \qquad (8.5)$$

$$x_{ma} = [\delta\phi_{ma} \ \delta\theta_{ma}]^T \qquad (8.6)$$

$$\dot{x}_{ma} = [b_{\phi_{ma}} \ b_{\theta_{ma}}]^T = \text{constant} \qquad (8.7)$$

At KF start, $x = 0_{12+2m}$.

2.3 SV time series

SV_{INR} time series (also called lookup tables) are generated at points spaced by Δt_i for image registration of section 6. This requires interpolation between SV_{KF} time series points determined by landmarks (or star measurements), time series points based on attitude telemetry (e.g., at one second interval) and FDS orbit, $SV_{ma,model}$, and $SV_{corr,model}$ time series (e.g., at one minute intervals). The SV_{KF} time series between measurements can be obtained as follows:

$$x(t_i) = A(\Delta t_i) x(t_0), \Delta t_i = t_i - t_0, t_0 \leq t_i \leq t_1 \qquad (9.1)$$

$$A(\Delta t_i) = \begin{bmatrix} A_{corr}(\Delta t_i) & 0_{6x6} & 0_{6x2m} \\ 0_{6x6} & A_{orb}(\Delta t_i) & 0_{6x2m} \\ 0_{2mx6} & 0_{2mx6} & A_{ma}(\Delta t_i) \end{bmatrix} \qquad (9.2)$$

$$A_{corr}(\Delta t_i) = \begin{bmatrix} I_{3x3} & I_{3x3}\Delta t_i \\ 0_{3x3} & I_{3x3} \end{bmatrix} \qquad (9.3)$$

$A_{orb}(\Delta t_i)$ is obtained from the well-known Euler-Hill equations[12]

$$A_{orb}(\Delta t_i) = \begin{bmatrix} A_{11} & A_{12} \\ A_{21} & A_{22} \end{bmatrix} \qquad (9.4)$$

$$A_{11} = \begin{bmatrix} (4 - 3 C) & 0 & 0 \\ 6(S - \gamma) & 1 & 0 \\ 0 & 0 & C \end{bmatrix} \qquad (9.5)$$

$$A_{12} = \begin{bmatrix} \omega_e^{-1} S & 2 \omega_e^{-1}(1 - C) & 0 \\ -2\omega_e^{-1}(1 - C) & \omega_e^{-1}(4S - 3\gamma) & 0 \\ 0 & 0 & \omega_e^{-1}S \end{bmatrix} \quad (9.6)$$

$$A_{21} = \begin{bmatrix} 3 \omega_e S & 0 & 0 \\ 6\omega_e(C - 1) & 0 & 0 \\ 0 & 0 & -\omega_e S \end{bmatrix} \qquad (9.7)$$

$$A_{22} = \begin{bmatrix} C & 2 S & 0 \\ -2 S & (4C - 3) & 0 \\ 0 & 0 & C \end{bmatrix} \qquad (9.8)$$

$$C = \text{Cos } \gamma, \ \ S = \text{Sin } \gamma, \ \ \gamma = \omega_e\Delta t_i, \ \omega_e^{-1} = \frac{1}{\omega_e}.$$

For small Δt_i, C=1 and S= $\gamma = \omega_e\Delta t_i$,

$$A_{orb}(\Delta t_i) = \begin{bmatrix} I_{3x3} & I_{3x3}\Delta t_i \\ 0_{3x3} & I_{3x3} \end{bmatrix} \qquad (9.9)$$

Note that Euler-Hill equations used to model orbit and the contents in section 3.4 used to model thermoelastic angles lead to significant reduction of the number of landmarks processed by KF compared to using simple linear models that are only valid for short time.

$$A_{ma}(\Delta t_i) = \begin{bmatrix} I_{mxm} & I_{mxm}\Delta t_i \\ 0_{mxm} & I_{mxm} \end{bmatrix} \qquad (9.10)$$

m = number of imager internal misalignments.

For single mirror imager used for GOES I-P, COMS, MTSAT2 and in this paper, m=2. For two mirror imagers, the number of misalignments depend on the thermoelastic effect on pointing. The leading term was called Orthogonality (O_{ma}) by Kamel because it represents the deviation of the scanning axes from being perpendicular. Note that if only O_{ma} has significant effect on pointing [11], the number of misalignments m=1.

3. Image Navigation Using KF

Fig. 1 shows KF flow for the fundamental INR method. KF uses one landmark at a time to determine best (a-posteriori) state vector and covariance matrix estimate (x_1^+, P_1^+). KF is then re-initialized to make propagation always between t_0 and t_1 and estimation at t_1.
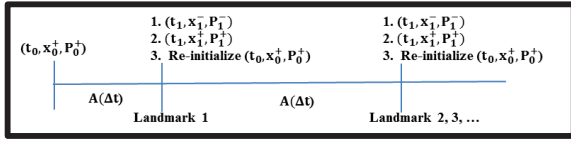

Fig. 1. Fundamental INR Method Kalman Filter

The 3-step process is as follows:

1. A-priori state vector and covariance matrix (x_1^-, P_1^-) are obtained from (x_0^+, P_0^+) using the transition matrix $A(\Delta t)$, $\Delta t = t_1 - t_0$ and error matrix $Q(\Delta t)$ obtained from system model. This first step is called SV and covariance matrix P propagation between two successive landmarks.

$$x_1^- = A(\Delta t)\, x_0^+ \qquad (10.1)$$
$$P_1^- = A(\Delta t)\, P_0^+ A(\Delta t)^T + Q(\Delta t) \qquad (10.2)$$

2. (x_1^+, P_1^+) is obtained from (x_1^-, P_1^-) and measurement model (Z, H, R). This second step is called SV and covariance matrix P estimation at t_1. Kalman assumed the relationship between x_1^+ and x_1^- is given by a form like least squares and determined associated Kalman gain matrix K and covariance matrix P:

$$x_1^+ = x_1^- - K\Delta Z, \ \Delta Z = Z - \bar{Z} \qquad (11.1)$$
$$K = P_1^- H^T (H P_1^- H^T + R)^{-1} \qquad (11.2)$$

$$P_1^+ = (I - KH)\, P_1^- (I - KH)^T + KRK^T \qquad (11.3)$$

The residual ΔZ is computed as follows:
- Compute SV_{INR} from x_1^- using sections 2.1 and 2.2.
- Compute landmark residuals using section 3.1.
- If landmark is rejected because residual is outside predetermined limit:
  ➢ Re-initialize KF:
    $(t_0,\ x_0^+, P_0^+) = (t_1, x_1^+, P_1^+) = (t_1, x_1^-, P_1^-)$.
  ➢ Skip estimation and go to next landmark.
- If landmark is accepted, compute x_1^+ using Eq. (11.1).
  Note that $(\Delta x_{corr}^+, \Delta x_{orb}^+, \Delta x_{ma}^+) = (x_{corr}^+, x_{orb}^+, x_{ma}^+) - (x_{corr}^-, x_{orb}^-, x_{ma}^-)$ obtained from Eq. (11.1) can cause jumps in level 1B images at t_1. This can be avoided by replacing $(\dot{x}_{corr}^+, \dot{x}_{orb}^+, \dot{x}_{ma}^+)$ [also obtained from Eq. (11.1) and given by Eqs. (8.3), (8.5) and (8.7)] with $(\dot{x}_{corr}^+, \dot{x}_{orb}^+, \dot{x}_{ma}^+) + (\Delta x_{corr}^+, \Delta x_{orb}^+, \Delta x_{ma}^+)/\delta t$, where, δt = delta time to next landmark or next KF point. After this slope adjustment, set $(x_{corr}^+, x_{orb}^+, x_{ma}^+) = (x_{corr}^-, x_{orb}^-, x_{ma}^-)$ at t_1.

3. The third step is to re-initialize KF by setting $(t_0,\ x_0^+, P_0^+) = (t_1, x_1^+, P_1^+)$ to start the next cycle from t_0 to t_1 and compute SV_{INR} from x_1^+ using section 2. This is needed for section 6.

3.1 KF landmark residual computation
The landmark residuals $\Delta Z = Z - \bar{Z}$ are computed from the next two subsections.

3.1.1 Actual landmark measurement $\bar{Z}$
In view of Fig. 2, we get:

$$\vec{R}_{To} = \vec{T} - \vec{R}_{So} \qquad (12.1)$$

Using vector components in GEOS coordinates, we get:

$$\vec{R}_{To} = (R_e + h)\begin{bmatrix} C_{L_T}S_{\Delta\lambda_T} \\ -S_{L_T} \\ -C_{L_T}C_{\Delta\lambda_T} \end{bmatrix} - R_{so}\begin{bmatrix} 0 \\ 0 \\ -1 \end{bmatrix}$$
$$= R_{To}\begin{bmatrix} C_{\bar{N}_{GEOS}}S_{\bar{E}_{GEOS}} \\ -S_{\bar{N}_{GEOS}} \\ C_{\bar{N}_{GEOS}}C_{\bar{E}_{GEOS}} \end{bmatrix} \qquad (12.2)$$

$$R_e = R_{eo}(1 + aS_{L_T}^2)^{-\frac{1}{2}} \cong R_{eo}(1 - f S_{L_T}^2) \qquad (12.3)$$
$$\Delta\lambda_T = \lambda_T - \lambda_{so},\ a = (1 - f)^{-2} - 1 \cong 2f \qquad (12.4)$$
This leads to:
$$R_{To} = \sqrt{R_{so}^2 + (R_e + h)^2 - 2R_{so}(R_e + h)C_{L_T}C_{\Delta\lambda_T}}$$
$$\bar{E}_{GEOS} = \text{Arc tan}\left[\frac{(R_e + h)C_{L_T}S_{\Delta\lambda_T}}{R_{so} - (R_e + h)C_{L_T}C_{\Delta\lambda_T}}\right] \qquad (13.1)$$
$$\bar{N}_{GOES} = \text{Arc sin}\left[\frac{(R_e + h)S_{L_T}}{R_{To}}\right] \qquad (13.2)$$
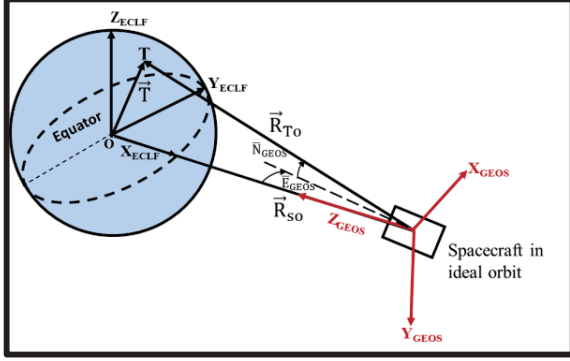$$\bar{Z} = \begin{bmatrix} \bar{E}_{GEOS} \\ \bar{N}_{GOES} \end{bmatrix} \qquad (13.3)$$

Fig. 2. ECLF to GEOS Geometry

3.1.2 Estimated landmark measurement Z

Transformation of landmark (E_{LRF}, N_{LRF}) coordinates to (E_{GEOS}, N_{GEOS}) coordinates is obtained in the next 4 subsections:

3.1.2.1 $\hat{U}_{IIRF}$ and $\hat{R}_{IIRF}$ computation

For single mirror instruments

$$E_{IIRF} = E_{LRF} - (\phi_{ma}S_{N_{LRF}} + \theta_{ma}C_{N_{LRF}}) \qquad (14.1)$$
$$N_{IIRF} = N_{LRF} - (\phi_{ma}C_{N_{LRF}} - \theta_{ma}S_{N_{LRF}})/C_{E_{LRF}} \quad (14.2)$$
(E_{LRF}, N_{LRF}) = determined landmark (EW, NS) angles.

To get (E_{LRF}, N_{LRF}) from (E_{IIRF}, N_{IIRF}) for inverse transformation, two iterations of Eqs. (14.1) and (14.2) may be needed starting with $(E_{LRF}, N_{LRF}) = (E_{IIRF}, N_{IIRF})$.

The unit vector $\hat{U}_{IIRF}$ components in IIRF coordinates is obtained by a rotation N_{IIRF} about X-axis followed by a rotation E_{IIRF} about the new Y-axis. This leads to:

$$\hat{U}_{IIRF} = \begin{bmatrix} S_{E_{IIRF}} \\ -C_{E_{IIRF}} S_{N_{IIRF}} \\ C_{E_{IIRF}} C_{N_{IIRF}} \end{bmatrix} \qquad (14.3)$$

The unit vector $\hat{R}_{IIRF}$ components in GEOS is given by:
$$\hat{R}_{IIRF} = C_{IIRF}^{GEOS} \hat{U}_{IIRF}$$
$$= [\hat{R}_{GEOS,x} \quad \hat{R}_{GEOS,y} \quad \hat{R}_{GEOS,z}]^T \qquad (14.4)$$
Note that for inverse transformation, use:
$$\hat{U}_{IIRF} = C_{GEOS}^{IIRF} \hat{R}_{IIRF}, \quad C_{GEOS}^{IIRF} = [C_{IIRF}^{GEOS}]^T \qquad (14.5)$$

3.1.2.2 IIRF to GEOS transformation matrix computation

Transformation from IIRF to GEOS is 3-1-2 type rotation and can be obtained from Appendix E, Table E-1, Ref. 13) by replacing (ϕ, θ, ψ) with $(\psi_C, \phi_C, \theta_C)$:
$$C_{IIRF}^{GEOS}$$
$$= \begin{bmatrix} C_\theta C_\psi - S_\theta S_\phi S_\psi & C_\theta S_\psi + S_\theta S_\phi C_\psi & -S_\theta C_\phi \\ -S_\psi C_\phi & C_\psi C_\phi & S_\phi \\ S_\theta C_\psi + C_\theta S_\phi S_\psi & S_\theta S_\psi - C_\theta S_\phi C_\psi & C_\phi C_\theta \end{bmatrix}_C$$
$$\cong \begin{bmatrix} 1 & \psi_C & -\theta_C \\ -\psi_C & 1 & \phi_C \\ \theta_C & -\phi_C & 1 \end{bmatrix} \qquad (15.1)$$

In view of Eqs. (3), (4), and (6) we get:

$$SV_C = \begin{bmatrix} \phi_C \\ \theta_C \\ \psi_C \end{bmatrix} = SV_{ACF} + SV_{corr} \qquad (15.2)$$

$$SV_{ACF} = SV_{ORF} + SV_{att} \qquad (15.3)$$

$$SV_{ACF} = \begin{bmatrix} \phi \\ \theta \\ \psi \end{bmatrix}, SV_{corr} = \begin{bmatrix} \phi_{corr} \\ \theta_{corr} \\ \psi_{corr} \end{bmatrix} \qquad (15.4)$$

$$SV_{ORF} = \begin{bmatrix} \phi_{orb} \\ \theta_{orb} \\ \psi_{orb} \end{bmatrix}, SV_{att} = \begin{bmatrix} \phi_{att} \\ \theta_{att} \\ \psi_{att} \end{bmatrix} \qquad (15.5)$$

3.1.2.3 R_{IIRF} computation

In view of Fig. 3 and Eq. (14.4), we get:
$$\vec{T} = \vec{R}_S + \vec{R}_{IIRF} \qquad (16.1)$$

$$(R_e + h) \begin{bmatrix} C_{L_T}S_{\Delta\lambda_T} \\ -S_{L_T} \\ -C_{L_T}C_{\Delta\lambda_T} \end{bmatrix} = R_s \begin{bmatrix} C_{L_s}S_{\Delta\lambda_s} \\ -S_{L_s} \\ -C_{L_s}C_{\Delta\lambda_s} \end{bmatrix}$$
$$+ R_{IIRF} \begin{bmatrix} \hat{R}_{GEOS,x} \\ \hat{R}_{GEOS,y} \\ \hat{R}_{GEOS,z} \end{bmatrix} \qquad (16.2)$$

R_{IIRF} can be obtained from Eq. (16.1) as follows:
$$|\vec{T}| = |\vec{R}_S + \vec{R}_{IIRF}| \qquad (17.1)$$
$$(R_e + h)^2 = R_{IIRF}^2 + R_S^2 - 2R_{IIRF}R_sC_{\alpha_s} \qquad (17.2)$$
$C_{\alpha_s} = -$dot product of unit vectors $\hat{R}_s$ and $\hat{R}_{IIRF}$
$$= -\hat{R}_{GEOS,x}C_{L_s}S_{\Delta\lambda_s} + \hat{R}_{GEOS,y}S_{L_s} + \hat{R}_{GEOS,z}C_{L_s}C_{\Delta\lambda_s}$$
Solution of the quadratic Eq. (17.2) leads to:
$$R_{IIRF} = R_S/r \qquad (17.3)$$
$$r = \left\{ C_{\alpha_s} - \sqrt{C_{\alpha_s}^2 - C_{\alpha_{so}}^2} \right\}^{-1}$$
$$C_{\alpha_{so}}^2 = 1 - [(R_e + h)/R_s]^2 \qquad (17.4)$$

Note that r is the same as $A(\alpha)$ in Ref. 1) and r in Ref. 10) and it is called earth curvature by Kamel because its value is dependent on Earth curvature.
R_e is obtained from Eq. (12.3) with S_{L_T} from the middle row of Eq. (16.2):
$$S_{L_T} = R_S(S_{L_s} - \frac{\hat{R}_{GEOS,y}}{r})/(R_e + h) \qquad (17.5)$$

Note that because $S_{L_T}^2$ is multiplied by small number in Eq. (12.3), one or two iterations using Eqs. (12.3), (17.4) and (17.5), starting with $R_e = R_{eo}$ in Eqs. (17.4) and (17.5), should be sufficient to get accurate values for R_e and r.
Note also that if $C_{\alpha_s}^2 < C_{\alpha_{so}}^2$, $\sqrt{C_{\alpha_s}^2 - C_{\alpha_{so}}^2}$ in Eq. (17.4) is imaginary indicating that the image pixel (E_{LRF}, N_{LRF}) corresponds to a point outside earth and (E_{GEOS}, N_{GEOS}) transition from earth to space will be undefined. This can be avoided if a fictitious earth with $C_{\alpha_{so}} = C_{\alpha_s}$ is used in Eq. (17.4) for the space portion of the earth images. In this case, Eqs. (17.3) and (17.4) lead to :
$$r = \frac{1}{C_{\alpha_s}}, R_{IIRF} = R_S C_{\alpha_s} \qquad (17.6)$$
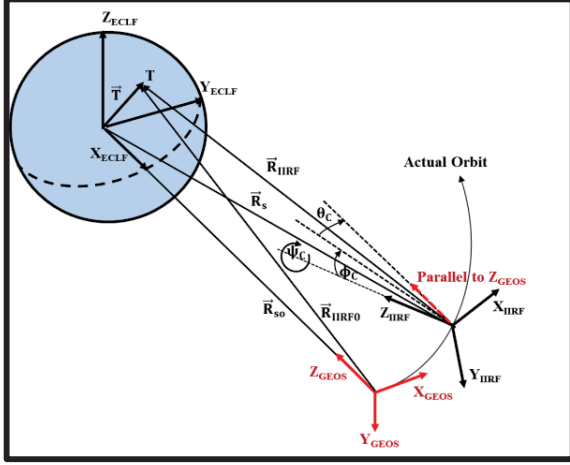
4

Fig. 3. Image Navigation Geometry

3.1.2.4 GEOS coordinates computation

In view of Fig. 3, we get:

$$\vec{R}_{IIRF0} = \vec{R}_{IIRF} + \Delta\vec{R}_S \quad (18.1)$$

$\vec{R}_{IIRF}$ from Eqs. (14.4) and (17.3) or (17.6),

$$\Delta\vec{R}_S = \vec{R}_S - \vec{R}_{S0} = \begin{bmatrix} R_s C_{L_s} S_{\Delta\lambda_s} \\ -R_s S_{L_s} \\ R_{so} - R_s C_{L_s} C_{\Delta\lambda_s} \end{bmatrix} \quad (18.2)$$

(E_{GEOS}, N_{GEOS}) are obtained from Fig. 3 and Eqs. (18.1) and (18.2):

$$\begin{bmatrix} C_{N_{GEOS}} S_{E_{GEOS}} \\ -S_{N_{GEOS}} \\ C_{N_{GEOS}} C_{E_{GEOS}} \end{bmatrix} = \begin{bmatrix} \hat{R}_{GEOS0,x} \\ \hat{R}_{GEOS0,y} \\ \hat{R}_{GEOS0,z} \end{bmatrix} = \frac{\vec{R}_{IIRF} + \Delta\vec{R}_S}{|\vec{R}_{IIRF} + \Delta\vec{R}_S|} \quad (18.3)$$

$$E_{GEOS} = \text{Arc tan}\left[\frac{\hat{R}_{GEOS0,x}}{\hat{R}_{GEOS0,z}}\right] \quad (18.4)$$

$$N_{GOES} = -\text{Arc sin } \hat{R}_{GEOS0,y} \quad (18.5)$$

$$Z = \begin{bmatrix} E_{GEOS} \\ N_{GOES} \end{bmatrix} \quad (18.6)$$

Note that for star measurements, Z is obtained directly from Eq. (14.4) and section 3.1.2.3 skipped because $\Delta\vec{R}_S$ is insignificant compared to $\vec{R}_{IIRF}$ in Eq. (18.3).

3.2 KF initial conditions

t_0 = epoch time = UTC_0 at start of KF.

$x_0^+ = SV_{KF}$ at epoch $= 0_{12+2m}$

P_0^+ = error covariance matrix at epoch

$$= \begin{bmatrix} P_{corr,0} & 0_{6x6} & 0_{6x2m} \\ 0_{6x6} & P_{orb,0} & 0_{6x2m} \\ 0_{2mx6} & 0_{2mx6} & P_{ma,0} \end{bmatrix} \quad (19.1)$$

$$P_{corr,0} = \sigma_{corr,0}^2 \begin{bmatrix} I_{3x3} & 0_{3x3} \\ 0_{3x3} & 0_{3x3} \end{bmatrix} \quad (19.2)$$

$$P_{orb,0} = \sigma_{orb,0}^2 \begin{bmatrix} I_{3x3} & 0_{3x3} \\ 0_{3x3} & 0_{3x3} \end{bmatrix} \quad (19.3)$$

$$P_{ma,0} = \sigma_{ma,0}^2 \begin{bmatrix} I_{mxm} & 0_{mxm} \\ 0_{mxm} & 0_{mxm} \end{bmatrix} \quad (19.4)$$

$\sigma_{corr,0} \cong \sigma_{orbit,0} \cong \sigma_{ma,0} \cong 5.0E\text{-}05$ for simulation.

3.3 KF detailed computation (for each data block)

After level 1A data block is searched for landmarks and if no landmarks were found within the data block, go to end of block of Eq. (21). If landmarks were found, the determined landmarks (= LM_T) are time tagged. KF propagation process starts from (t_0, x_0^+, P_0^+) of the last event prior to the data block to the first (t_1, x_1^-, P_1^-) within the data block followed by (t_1, x_1^+, P_1^+) estimation and re-initialization as shown in Fig. 1. This process is repeated for all determined landmarks as follows:

For k=1 to LM_T do to **ENDFOR**

$$\Delta t = t_1 - t_0 \quad (20)$$

$t_1 = UTC_k$ time at landmark number k.

Propagation: From step number 1 of section 3.
Estimation: From step number 2 of section 3.
Re-initialize KF: From step number 3 of section 3.
ENDFOR

At end of data block, do the following:

$$\Delta t = t_1 - t_0 \quad (21)$$

$t_1 = UTC_{end}$ = time at end of data block

Propagation: From step number 1 of section 3.
Re-initialize KF:

$(t_0, x_0^+, P_0^+) = (t_1, x_1^+, P_1^+) = (t_1, x_1^-, P_1^-)$

Compute SV_{INR} from x_1^+ using section 2. This is needed for section 6.

If maneuver delta V is provided by FDS

At maneuver, do the following:

$$\Delta t = t_1 - t_0, \quad t_1 = UTC_{maneuver} = \text{maneuver time} \quad (22.1)$$

Propagation: From step number 1 of section 3.
Re-initialize KF:

$$x_1^+ = x_1^- + \Delta x \quad (22.2)$$

$$P_1^+ = P_1^- + \Delta P \quad (22.3)$$

$$\Delta x = \begin{bmatrix} 0_{1x9} & \frac{\Delta v_{FDS,r}}{R_{so}} & \frac{\Delta v_{FDS,\lambda}}{R_{so}} & \frac{\Delta v_{FDS,L}}{R_{so}} & 0_{1x2m} \end{bmatrix}^T \quad (22.4)$$

ΔP= diagonal terms 10 to 12 from delta v error analysis.

$$(t_0, x_0^+, P_0^+) = (t_1, x_1^+, P_1^+) \quad (22.5)$$

Compute SV_{INR} from x_1^+ using section 2. This is needed for section 6.

If orbit is provided by FDS instead of delta V

At orbit determination, do the following:

$$\Delta t = t_1 - t_0, \quad t_1 = UTC_{OD} = \text{orbit determination time} \quad (23.1)$$

Propagation: From step number 1 of section 3.
Re-initialize KF:

$$x_1^+ = x_1^- + \delta x \quad (23.2)$$

$$P_1^+ = P_1^- + \delta P \quad (23.3)$$

$$\delta x = \begin{bmatrix} 0_{1x6} & \delta\left(\frac{\Delta R_s}{R_{so}}\right) & \delta\Delta\lambda_s & \delta L_s & 0_{1x(3+2m)} \end{bmatrix}^T \quad (23.4)$$

$(\delta\Delta R_s, \delta\Delta\lambda_s, \delta L_s) = (R_{FDS}, \Delta\lambda_{FDS}, L_{FDS})^-$ before OD $- (R_{FDS}, \Delta\lambda_{FDS}, L_{FDS})^+$ after OD (23.5)

δP= diagonal terms 7 to 9 from OD error analysis.

$$(t_0, x_0^+, P_0^+) = (t_1, x_1^+, P_1^+) \qquad (23.6)$$

Compute SV_{INR} from x_1^+ using section 2. This is needed for section 6.

Transition matrix A: From section 2.3.

Process noise covariance matrix Q:
From Eqs. (13-83) and (13-89) of Ref. 13, we get:

$$Q(\Delta t) = V_0 + V\Delta t + \frac{1}{2}\left[F_x V + VF_x^T\right]\Delta t^2$$
$$+ \frac{1}{3}F_x V F_x^T \Delta t^3 \qquad (24.1)$$

$$V_0 = \begin{bmatrix} V_{corr,0} & 0_{6x6} & 0_{6x2m} \\ 0_{6x6} & V_{orb,0} & 0_{6x2m} \\ 0_{2mx6} & 0_{2mx6} & V_{ma,0} \end{bmatrix} \qquad (24.2)$$

$$V = \begin{bmatrix} V_{corr} & 0_{6x6} & 0_{6x2m} \\ 0_{6x6} & V_{orb} & 0_{6x2m} \\ 0_{2mx6} & 0_{2mx6} & V_{ma} \end{bmatrix} \qquad (24.3)$$

Where

$$V_{y,0} = \begin{bmatrix} \sigma_{e,y}^2 I_{3x3} & 0_{3x3} \\ 0_{3x3} & 0_{3x3} \end{bmatrix}, V_y \begin{bmatrix} \sigma_{v,y}^2 I_{3x3} & 0_{3x3} \\ 0_{3x3} & \sigma_{u,y}^2 I_{3x3} \end{bmatrix} \quad (24.4)$$

y = corr, orb, or ma. For ma, 3 replaced by m.
σ_e = measurement white noise standard deviation, rad.
σ_v = random walk standard deviation, $rad/sec^{1/2}$.
σ_u = rate random walk standard deviation, $rad/sec^{3/2}$.

$$F_x = \begin{bmatrix} F_{corr} & 0_{6x6} & 0_{6x2m} \\ 0_{6x6} & F_{orb} & 0_{6x2m} \\ 0_{2mx6} & 0_{2mx6} & F_{ma} \end{bmatrix} \qquad (25.1)$$

Where,

$$F_{corr} = \begin{bmatrix} 0_{3x3} & I_{3x3} \\ 0_{3x3} & 0_{3x3} \end{bmatrix} \qquad (25.2)$$

F_{orb} from Euler-Hill equations:

$$F_{orb} = \begin{bmatrix} 0_{3x3} & I_{3x3} \\ \omega_e^2 F_{21} & 2\omega_e F_{22} \end{bmatrix} \cong \begin{bmatrix} 0_{3x3} & I_{3x3} \\ 0_{3x3} & 0_{3x3} \end{bmatrix}$$

$$F_{21} = \begin{bmatrix} 3 & 0 & 0 \\ 0 & 0 & 0 \\ 0 & 0 & -1 \end{bmatrix}, F_{22} = \begin{bmatrix} 0 & 1 & 0 \\ -1 & 0 & 0 \\ 0 & 0 & 0 \end{bmatrix} \qquad (25.3)$$

$$F_{ma} = \begin{bmatrix} 0_{mxm} & I_{mxm} \\ 0_{mxm} & 0_{mxm} \end{bmatrix} \qquad (25.4)$$

This leads to the closed form noise covariance matrix:

$$Q(\Delta t) = \begin{bmatrix} Q_{corr} & 0_{6x6} & 0_{6x2m} \\ 0_{6x6} & Q_{orb} & 0_{6x2m} \\ 0_{2mx6} & 0_{2mx6} & Q_{ma} \end{bmatrix} \qquad (25.5)$$

$$Q_y = $$
$$\begin{bmatrix} \left(\sigma_{e,y}^2 + \sigma_{v,y}^2 \Delta t + \frac{1}{3}\sigma_{u,y}^2\Delta t^3\right) I_{3x3} & \frac{1}{2}\sigma_{u,y}^2\Delta t^2 I_{3x3} \\ \frac{1}{2}\sigma_{u,y}^2\Delta t^2 I_{3x3} & \sigma_{u,y}^2 \Delta t\, I_{3x3} \end{bmatrix} \quad (25.6)$$

Where,
y = corr, orb, or ma. For ma, I_{3x3} is replaced by I_{mxm}.

Note that the first element of the above matrix is the same as Eq. (7-143) in Ref 13).

The sigma values can be computed using Eq. (25.6), SV_{INR} error analysis and estimate of time between measurements. For COMS simulation, this leads to:
$(\sigma_{e,corr}, \sigma_{e,orb}, \sigma_{e,ma})$= (1.942E-07,0,0).
$(\sigma_{v,corr}, \sigma_{v,orb}, \sigma_{v,ma})$ = (4.8E-07, 0, 1.3E-09).
$(\sigma_{u,corr}, \sigma_{u,orb}, \sigma_{u,ma})$ = (4.8E-10, 9.3E-13, 2.3E-11).

Landmark measurement noise covariance matrix R:
$R_k = \sigma_M^2 I_{2x2}$
σ_M = measurement noise calculated from landmark determination error analysis (= 0.1 pixel for simulation).

Landmark location sensitivity matrix H:
H is determined from $\left(\frac{\partial Z}{\partial x}\right)_{x=0}$ where Z is the estimated landmark location measurement from section 3.1.2 using the linear representation of C_{IIRF}^{GEOS} of Eq. (15.1). After some laborious algebraic manipulation, we get:
H = 2x(12 + 2m) matrix given by:

$$H = \left(\frac{\partial Z}{\partial x}\right)_{x=0} = [H_{corr} \quad H_{orb} \quad H_{ma}] \qquad (26.1)$$

Where,

$$H_{corr} = -\begin{bmatrix} T_{\bar{N}}S_{\bar{E}} & 1 & T_{\bar{N}}C_{\bar{E}} & 0_{1x3} \\ C_{\bar{E}} & 0 & -S_{\bar{E}} & 0_{1x3} \end{bmatrix} \qquad (26.2)$$

For Spacecraft x axis parallel to earth equator (e.g., COMS):

$$H_{orb} = -\begin{bmatrix} 0 & 1 & T_{\bar{N}}S_{\bar{E}} & 0_{1x3} \\ 0 & 0 & C_{\bar{E}} & 0_{1x3} \end{bmatrix} +$$
$$\bar{r}\begin{bmatrix} \frac{S_{\bar{E}}}{C_{\bar{N}}} & \frac{C_{\bar{E}}}{C_{\bar{N}}} & 0 & 0_{1x3} \\ C_{\bar{E}}\,S_{\bar{E}} & -S_{\bar{E}}S_{\bar{N}} & C_{\bar{N}} & 0_{1x3} \end{bmatrix} \qquad (26.3)$$

For Spacecraft x axis parallel to orbit plane (e.g., GOES I-M):
Replace $\begin{bmatrix} 0 & 1 & T_{\bar{N}}S_{\bar{E}} & 0_{1x3} \\ 0 & 0 & C_{\bar{E}} & 0_{1x3} \end{bmatrix}$ by

$$\begin{bmatrix} 0 & 1 & T_{\bar{N}}S_{\bar{E}} & 0_{1x2} & T_{\bar{N}}C_{\bar{E}}/\omega_e \\ 0 & 0 & C_{\bar{E}} & 0_{1x2} & -S_{\bar{E}}/\omega_e \end{bmatrix}$$

$$\bar{r} = \left(C_{\bar{\alpha}_s} - \sqrt{C_{\bar{\alpha}_s}^2 - 1 + ((R_e + h)/R_{so})^2}\right)^{-1} \quad (26.4)$$

$$C_{\bar{\alpha}_s} = Cos\bar{\alpha}_s = C_{\bar{N}}C_{\bar{E}} \qquad (26.5)$$

$T_{\bar{N}} = Tan\,\bar{N}_{GEOS}, S_{\bar{N}} = Sin\,\bar{N}_{GEOS}, C_{\bar{N}} = Cos\,\bar{N}_{GEOS}$
$S_{\bar{E}} = Sin\,\bar{E}_{GEOS}, C_{\bar{E}} = Cos\bar{E}_{GEOS}$
$(\bar{E}_{GEOS}, \bar{N}_{GEOS})$ = landmark location from Eq. (13.4).
R_e = earth radius at landmark location from Eq. (12.3).
h= landmark altitude.

For star measurements, r = 0 and H_{orb} becomes insensitive to orbit translational part ($\delta R/R_{so}$, $\delta\lambda$, δL). Therefore, stars cannot be used to refine orbit and, therefore, orbit refinement must be deleted from KF as described in section 5.1.

For single mirror imaging systems:

$$H_{ma} = \begin{bmatrix} C_{11} & C_{12} & 0 & 0 \\ C_{21} & C_{22} & 0 & 0 \end{bmatrix} \qquad (26.6)$$

$$C_{11} = -\frac{C_{22}}{C_{\overline{N}}}, C_{12} = \frac{C_{21}}{C_{\overline{N}}},$$

$$C_{21} = \frac{S_{\overline{E}} - C_{\overline{N}}}{1 - C_{\overline{N}}S_{\overline{E}}}, C_{22} = \frac{S_{\overline{N}}C_{\overline{N}}}{1 - C_{\overline{N}}S_{\overline{E}}} \qquad (26.7)$$

H_{ma} for two mirror imaging systems to be investigated in the future.

3.4 Thermoelastic model time series

The thermoelastic $SV_{ma,model}$ and $SV_{corr,model}$ time series can be obtained from Eqs. (2.1) and (3.1) as follows:

1. Create daily time series at, e.g., one-minute interval for, e.g., seven days using interpolation of SV_{ma} and SV_{corr} data at time $t_{i,n}$, i =1, 2, …, 1440 and n=1, 2…,7.

2. The $SV_{ma,model}$ $(t_{i,n})$ and $SV_{corr,model}$ $(t_{i,n})$ for the next day (n=8) are obtained by averaging the last seven days of $SV_{ma}(t_{i,n})$ and $SV_{corr}(t_{i,n})$ data:

$$SV_{ma,model}(t_{i,8}) = \frac{1}{7}\sum_{n=1}^{n=7} SV_{ma}(t_{i,n}) \qquad (27.1)$$

$$SV_{corr,model}(t_{i,8}) = \frac{1}{7}\sum_{n=1}^{n=7} SV_{corr}(t_{i,n}) \qquad (27.2)$$

Note that $SV_{ma,model}$ and $SV_{corr,model}$ are initially determined by analysis or set to zero.

3. Repeat above process once a day using one-day sliding window.

4. COMS Simulation Results

A hundred landmarks distributed over earth and COMS imaging schedule were used in the simulation[14-15]. The true $\overline{SV}_{INR}$ is calculated using eccentricity =0.0001, inclination = 0.05°, $SV_{ma,model}$ and $SV_{corr,model}$ amplitudes = 100 µrad, with 24-hour period, and attitude amplitude = 300 µrad with 2.4-hour period. The maneuver delta V times obtained from Ref. 16), Figure 8, and magnitudes from Ref. 17), Tables 2. The estimated SV_{INR} are shown in Fig. 4 for seven days and is computed using section 3.3 based on $SV_{ma,model}$ and $SV_{corr,model}$ errors =10 µrad, FDS maneuver delta V errors from Ref. 17), Table 3 or FDS orbit determination error from Table 7. Fig. 5 shows SV errors $\delta SV = \overline{SV}_{INR} - SV_{INR}$. Fig. 6 shows residual errors computed using section 3.1. The simulated landmarks are obtained using the true $\overline{SV}_{INR}$ to transfer $(\overline{E}_{GEOS}, \overline{N}_{GEOS})$ to $(\overline{E}_{LRF}, \overline{N}_{LRF})$ based on section 3.1.2 inverse transformation. The estimated (E_{LRF}, N_{LRF}) are then obtained from actual $(\overline{E}_{LRF}, \overline{N}_{LRF})$ by adding a random normal distribution landmark determination error with σ_M = 2.8E-06 radians for visible landmarks and σ_M= 11.2E-06 radians for IR landmarks. Simulation was also successfully used to stress test the fundamental method for cases using eccentricity = 0.001, inclination = 0.5°, $SV_{ma,model}$ and $SV_{corr,model}$ amplitudes = 1000 µrad with errors =100 µrad and only IR landmarks.

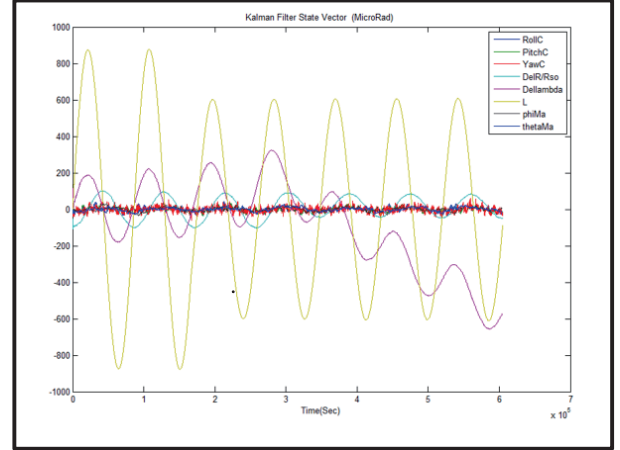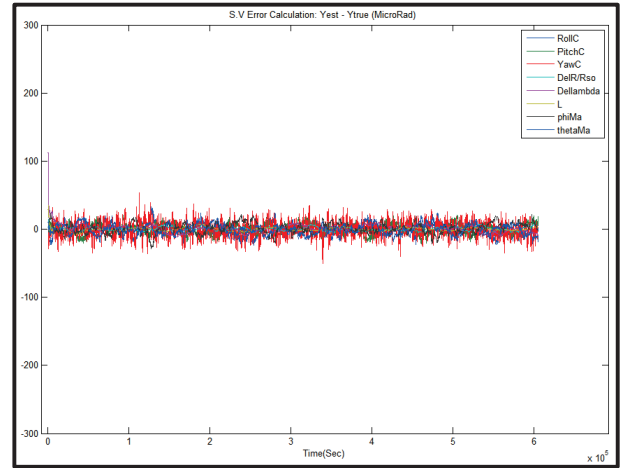Fig. 4. KF State Vector

Fig. 5 SV Errors $\delta SV = SV_{INR} - \overline{SV}_{INR}$.
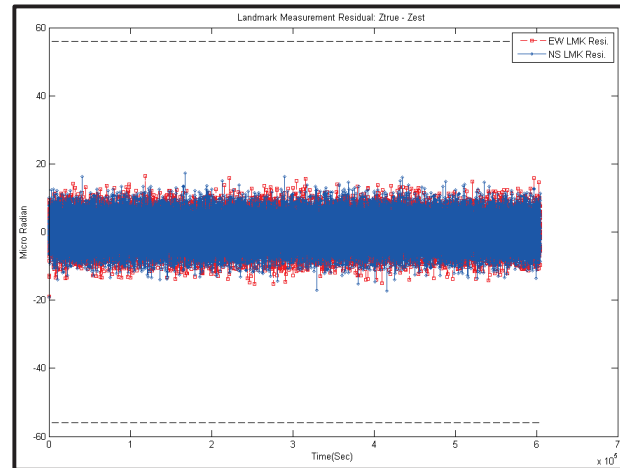

Fig. 6. Landmarks Measurement Residuals

5. Adaptation to Other INR System Measurements

5.1 Systems based on star and landmark measurements

For stars:

- KF refinements $(\delta R_s/R_{so}, \delta\lambda_s, \delta L_s) = (0,0,0)$ and $(x_{orb}, \dot{x}_{orb})$ deleted from KF state vector.
- Rows and columns associated with $P_{orbit,0}$ A_{orbit}, P_{orbit} and F_{orbit} deleted from P_0^+, A, V, V_0, and F_x.
- H_{orbit} deleted from H.

In this case:

➢ one star per minute or 3 stars per 5 minutes are sufficient to determine x_{corr} and x_{ma}.
➢ Kalman SV dimension = 6+2m instead of 12+2m.
➢ KF detailed computation is like the fundamental method with landmarks replaced by stars.

For landmarks:

- Use KF for orbit refinements $(\delta R_s/R_{so}, \delta\lambda_s, \delta L_s)$ using the above deleted items.
  In this case:

➢ Few landmarks (e.g.,10 well distributed landmarks over earth) are sufficient to determine $(x_{orb}, \dot{x}_{orb})$.
➢ Kalman SV dimension = 6 instead of 12+2m.

5.2 Systems based on star measurements and no landmarks

- KF same as in section 5.1 for stars. In this case, the orbit must be provided by FDS or GPS.

5.3 Systems based on spacecraft inertial angular rate telemetry

The $(\omega_{sx}, \omega_{sy}, \omega_{sz})$ telemetry represent inertial angular rate along ACF axes in the form of time series spaced at Δt_{att} (e.g., 0.01 seconds) inserted in the imager wideband data. The rates $\dot{SV}_{ACF}$ of Eq. (15.3) can be obtained from $(\omega_{sx}, \omega_{sy}, \omega_{sz})$ using Fig. 3 with IIRF replaced by ACF. Starting with $\dot{\theta} + \omega_e$ about $-Y_{GEOS}$ axis followed by $\dot{\phi}$ about the new $-X$ axis followed by $\dot{\psi}$ about $-Z_{ACF}$ axis and using Eqs. (14.5) and (15.1), we get:

$$\begin{bmatrix} \omega_{sx} \\ \omega_{sy} \\ \omega_{sz} \end{bmatrix} = -\dot{\psi}\begin{bmatrix} 0 \\ 0 \\ 1 \end{bmatrix} - \dot{\phi}\begin{bmatrix} C_\psi \\ S_\psi \\ 0 \end{bmatrix} - (\dot{\theta} + \omega_e)\begin{bmatrix} -S_\psi C_\phi \\ C_\psi C_\phi \\ S_\phi \end{bmatrix} \quad (28.1)$$

This leads to:

$$\dot{SV}_{ACF} = \begin{bmatrix} \dot{\phi} \\ \dot{\theta} \\ \dot{\psi} \end{bmatrix} = -\begin{bmatrix} \omega_{sy}S_\psi + \omega_{sx}C_\psi \\ \omega_e + (\omega_{sy}C_\psi - \omega_{sx}S_\psi)/C_\phi \\ \omega_{sz} - (\omega_{sy}C_\psi - \omega_{sx}S_\psi)S_\phi/C_\phi \end{bmatrix}$$

$$\cong -\begin{bmatrix} \omega_{sx} + \omega_{sy}\psi \\ \omega_{sy} + \omega_e - \omega_{sx}\psi \\ \omega_{sz} - \omega_{sy}\phi \end{bmatrix} \quad (28.2)$$

Note that Eq. (28.2) can also be obtained from Ref. 13), Appendix E Table E-2 for 2-1-3 type rotation by replacing (ϕ, ψ) with $-(\phi, \psi)$ and $(\omega_I, \omega_J, \omega_K)$ with $(\omega_{sy}, \omega_{sx}, \omega_{sz})$ on the right side of the equation and replacing $(\dot{\phi}, \dot{\theta}, \dot{\psi})$ with $-(\dot{\theta} + \omega_e, \dot{\phi}, \dot{\psi})$ on the left side of the equation.

Now, the SV_C time series spaced by Δt_{att} over $\Delta t = t_1 - t_0$ is computed as follows:
Let $j = \text{Integer}(\Delta t/\Delta t_{att})$, $\tau_i = t_0 + i\,\Delta t_{att}$
For $i = 1, \ldots, j$ plus final step from τ_j to t_1

$$SV_C(\tau_i) = SV_C(\tau_{i-1}) + \dot{SV}_C(\tau_{i-1})\Delta t_{att} \quad (28.3)$$

Where, $\dot{SV}_C(\tau_{i-1})$ computed from Eqs. (15.2) and (3.2)

$$\dot{SV}_C(\tau_{i-1}) = \dot{SV}_{ACF}(\tau_{i-1}) + \dot{SV}_{corr,model}(\tau_{i-1}) + \dot{x}_{corr}(\tau_{i-1}) \quad (28.4)$$

With $\dot{SV}_{ACF}(\tau_{i-1})$ computed from Eq. (28.2) using (ϕ, ψ) from Eqs. (15.2) and (3.2)

$$SV_{ACF}(\tau_{i-1}) = SV_C(\tau_{i-1}) - SV_{Corr,model}(\tau_{i-1}) - x_{corr}(\tau_{i-1}) \quad (28.5)$$

$SV_{corr,model}$ and its slope $\dot{SV}_{corr,model}$ obtained from section 3.4 and $(x_{corr}, \dot{x}_{corr})$ determined by KF and defined in Eqs. (8.2) and (8.3).

At KF start (see sections 3.2 and 3.4):

$$SV_{KF} = 0_{12+2m} \text{ and } SV_{corr,model} = 0_3 \quad (29.1)$$

In view of Eqs. (15.2), (15.3), and (6.1) to (6.3)

$$SV_C(t_0) = SV_{ACF}(t_0) = SV_{ORF}(t_0) + SV_{att}(t_0) \quad (29.2)$$

$$SV_{att}(t_0) \text{ from telemetry or} = 0_3. \quad (29.3)$$

$$\dot{SV}_C(t_0) = \dot{SV}_{ACF}(t_0) \text{ from Eq. (28.2).} \quad (29.4)$$

At KF re-initialization (see Fig. 1):

$$SV_C(t_0) = SV_C(t_1) \text{ from Eq. (28.3)} \quad (29.5)$$

$$\dot{SV}_C(t_0) = \dot{SV}_C(t_1) \text{ from Eq. (28.4)} \quad (29.6)$$

$$SV_{ACF}(t_0) = SV_{ACF}(t_1) \text{ from Eq. (28.5)} \quad (29.7)$$

$$\dot{SV}_{ACF}(t_0) = \dot{SV}_{ACF}(t_1) \text{ from Eq. (28.2)} \quad (29.8)$$

Note that $\dot{SV}_{ACF}$ of Eq. (28.4) is corrected by $\dot{x}_{Corr}$ determined by KF to compensate for gyro drift and ACF to IIRF thermoelastic attitude change.

6. Image Registration Using Resampling

Image registration requires two steps. The first step is to transfer level 1A (column, line) pixel indices (c, ℓ) to $(c', \ell') = (c, \ell) + (\Delta c, \Delta\ell)_{c,\ell}$ in the GEOS fixed frame. The second step is to resample (c', ℓ') pixels to generate level 1B data block (see, e.g., Ref. 18). The first step can be performed using section 3.1.2 algorithm to determine $(\Delta c, \Delta\ell)_{c,\ell}$ from $(\Delta E, \Delta N)_{c,\ell} = (E_{GEOS}, N_{GEOS})_{c,\ell} - (E_{LRF}, N_{LRF})_{c,\ell}$ divided by pixel size. Index ℓ and N_{LRF} are fixed over pixel line and index c and E_{LRF} are fixed over pixel column. The SV_{INR} time series needed for (c, ℓ) to (c', ℓ') transformation is obtained from section 2.3. The processing time of this transformation is significantly reduced by computing $(\Delta C, \Delta L)_{C,L}$ for a subset of pixels (C, L) uniformly distributed over the level 1A (c, ℓ) array. The $(\Delta c, \Delta\ell)_{c,\ell}$ for the remaining pixels are then computed by EW and NS linear interpolation between the $(\Delta C, \Delta L)_{C,L}$ subset. Note that the number of (C, L) pixel subset is obtained by analysis of SV_{INR} and attitude jitter effects on registration error.

Note also that level 1A block should be slightly larger than level 1B block to account for the shift caused by orbit, attitude, and misalignment variation over time.

7. Conclusion

INR and KF state vectors suitable for the new INR method were defined. The fundamental method is based on landmark measurements to determine orbit, attitude correction angles, and imager misalignments with maneuvers delta V (or orbit with coarse accuracy) provided by FDS. The method was proven by simulation. Adaptation of this method to other INR systems and an algorithm for transferring pixels from LOS to GEOS frame needed for pixel data resampling are presented.

Acknowledgments

References

1. Kamel A A: GOES Image Navigation and Registration System, SPIE, 2812, pp 766-776, 1996.
2. Lu F et al: Image Navigation for the FY2 Geosynchronous Meteorological Satellite, 1 July 2008.
3. Woo J et al.: Analysis of COMS MI Image Navigation and Registration Performance, ISRS 2-4 November 2011.
4. Chambon T et al: On-ground evaluation of MTG Image Navigation and Registration (INR) performances, Proc. SPIE 8889, Sensors, Systems, and Next-Generation Satellites XVII, 88891J, 16 October 2013.
5. Okuyama A et al: Preliminary validation of Himawari-8/AHI navigation and calibration, 9 November 2015.
6. Kamel A A: Precise Spacecraft Camera Image Navigation and Registration, US patent #5,963,166, 5 October 1999.
7. Carr J L: Twenty-five years of INR, The Journal of Astronautical Sciences, Volume 57, pp 505-515, January 2009.
8. Harris J et al: Image Navigation and Registration improvements using GPS, Geoscience and Remote Sensing Symposium, 2009 IEEE International, IGARSS, Volume 3, pp 247-250, July 2009.
9. De Luccia F J et al: Image navigation and registration performance assessment tool set for the GOES-R Advanced Baseline Imager and Geostationary Lightning Mapper, 4 April 2016.
10. Virgilio V N: Geolocation of Remotely Sensed Pixels by Introspective Landmarking, US 8942421, 27 January 2015.
11. GOES Earth Location User's Guide (ELUG), DRL 504-11 Revision 1, Appendix C, NOAA, March 1998.
12. Sidi M J, Spacecraft Dynamics & Control, Cambridge University Press,1997.
13. Wertz J R: Spacecraft Attitude Determination and Control, D. Reidel Publishing, Hingham, Mass 1978, reprinted in 2000 by Kluwer Academic Publisher, Boston, Mass.
14. Final Technical Report: As part of the deliverables of the Contract for Technical COMS Technical Monitoring and Services, Contract No. KARI-13-0007, 18 April 2014.
15. Final Technical Report: As part of the deliverables of the Contract for Technical COMS Technical Monitoring and Services, Contract No. KARI-15-0012, 24 April 2015.
16. Lee B S et al: East-West Station-Keeping Maneuver Strategy for COMS Satellite Using Iterative Process. Advances in Space Research, the Official Journal of the Committee on Space Research (COSPAR), September 2010.
17. Hwang Y et al: Orbit Determination Accuracy improvement for Geostationary Single Station Antenna Tracking ETRI Journal, Volume 30, No. 6, December 2008.
18. Ormiston J P et al: GOES Advanced Baseline Imager – Ground Processing Development System, 5th GOES Users' Conference, 23 January 2008.